Influence of groundwater flow on thermochronometer-derived exhumation rates in the central Nepalese Himalaya

David M. Whipp, Jr. and Todd A. Ehlers

Appendix A: Numerical model setup

Thermal model

The thermal field for the central Nepal study region is calculated using a modified version of the 3D finite-element code FRACTure (Kohl and Hopkirk, 1995), similar to that implemented by Whipp et al. (2007). The 3D advection-diffusion equation is solved to thermal steady state using a Galerkin finite element scheme with implicit time stepping. The model domain is 84 x 140 x 50 km and the upper surface is a 250 m digital elevation model (DEM) of the area surrounding the Marsyandi River valley (Fig. DR1; resampled from Fielding et al., 1994). The top surface model has a fixed temperature boundary condition with a temperature of 28°C at 0 m and lapse rate of -7°C/km elevation increase. The base of the model has a constant flux boundary condition of 35 mW/m^2 and the other faces of the model have a zero flux boundary. Elements in Greater Himalayan Sequence (GHS), Lesser Himalayan Sequence (LHS), Indian Shield (IS) and Tibetan Sequence (TS) have assigned radiogenic heat production values of 1.9 μW/m^3, 0.8 μW/m^3, 0.8 μW/m^3 and 0.5 μW/m^3, respectively. The entire model domain uses a thermal conductivity value of 2.5 W/m/K. Thermal model parameters used in our simulations are summarized in Table DR1.

Tectonic (kinematic) model

The kinematic model prescribes a velocity field for elements within the model that reflects transport of material parallel to the active faults in the model domain (Fig. DR1b). Fault motion is partitioned between underthrusting (subduction) of the Indian Shield and overthrusting on the Main Frontal Thrust (MFT) and Main Central Thrust (MCT). The fault geometry is

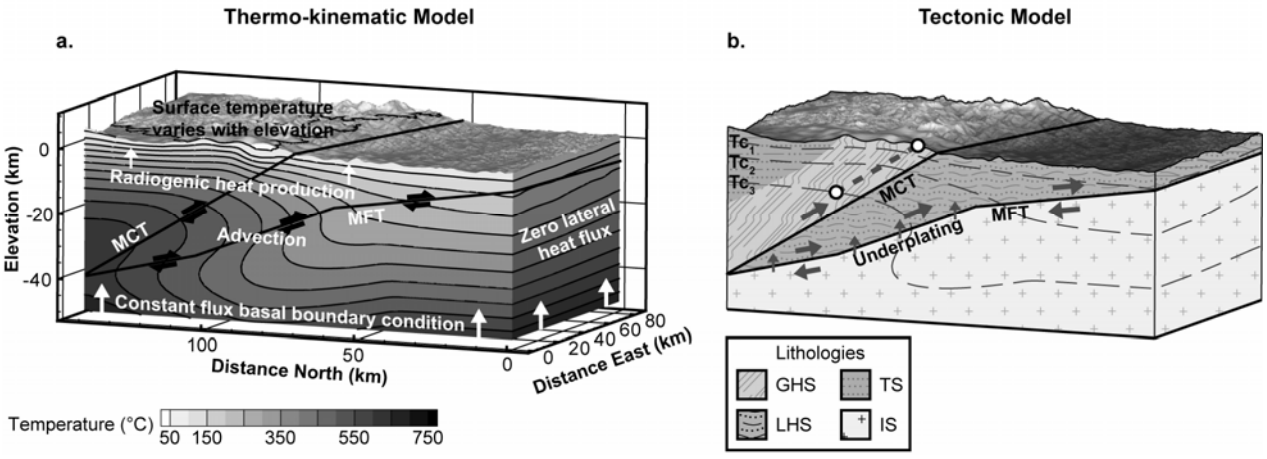

Figure DR1 – 3D block diagrams of the thermokinematic and tectonic models. (a) Example fluid-advective thermokinematic model illustrating the boundary conditions and thermal model components. The kinematic model has the Main Frontal Thrust (MFT) and Main Central Thrust (MCT) active (thick lines). Contoured temperatures (thin lines) show significant perturbation to the subsurface thermal field from the kinematic model and other thermal influences. (b) 3D block diagram of the tectonic model where slip is partitioned between the MCT and MFT (arrows show sense of motion on faults). Exhumation pathways (thick dashed line) parallel the faults and material is transferred into the overriding wedge via underplating (small vertical arrows). The exhumation pathway is for a thermochronometer sample sensitive to closure temperatures Tc_1–Tc_3 (white circles, thin dashed lines).

described in detail by Whipp et al. (2007). The horizontal convergence rate between India and Tibet is fixed at 20 mm/yr in the model, consistent with present-day geodetic measurements (Bilham et al., 1997; Larson et al., 1999). For the majority of the models 4 mm/yr of convergence is accommodated by the MFT, 2 mm/yr by the MCT and 14 mm/yr by subduction. The convergence rates are from the best-fit kinematic models identified by Whipp et al. (2007) from 397 different simulations. Because the model geometry does not change with time, the kinematic scenario generates a vertical exhumation (denudation) rate of ~2.5 mm/yr. For the models where the kinematics are varied, the MFT and MCT are active at convergence rates of 2–8 mm/yr and 1–4 mm/yr, respectively, generating denudation rates of 1.3–5.0 mm/yr.

Hydrologic model

The hydrologic model utilized in this study simulates the large-scale flow of a fluid (water) driven by pressure gradients resulting from variations in the water table elevation due to topography (Fig. DR2). Groundwater flow is driven by short and long wavelength topography. The primary effect in the upper crust is flow from ridges into adjacent valleys (Fig. DR2b). The other major circulation pattern is the flow from the Tibetan Plateau down toward the Indian foreland (Fig. DR2c). The superposition of both flows generates the observed thermal disturbance.

The surface boundary condition has the water table elevation set to mimic topography as an approximation of the true water table geometry. All other sides of the model have a zero flux boundary. The fluid in the model is set to behave like water with a temperature-dependent viscosity following the approaches of Smith and Chapman (1983) and pressure and temperature-dependent density (Phillips et al., 1981). Because heat transfer in the model is often dominated by fluid advection, streamline upwinding is used to stabilize the solution following the approach of Brooks and Hughes (1982). Other model parameters are summarized in Table DR1.

TABLE DR1. NUMERICAL MODEL PARAMETERS

Property/parameter	Input value
General model	
Model time step	10^5 yr
Horizontal node spacing	700 m
Average vertical node spacing	~1500 m
Model domain (x, y, z)	84 x 140 x 50 km
Thermal model†	
GHS heat production	1.9 μW/m^3
LHS/IS heat production	0.8 μW/m^3
TS heat production	0.5 μW/m^3
Thermal conductivity	2.5 W/m K
Rock specific heat	800 J/kg K
Rock density	2750 kg/m^3
Surface temperature	28 - (7 * z) ºC
Basal heat flow	35 mW/m^2
Kinematic model†	
India-Tibet convergence rate	20 mm/yr
MFT overthrusting rate	2–8 mm/yr
MCT cverthrusting rate	1–4 mm/yr
Hydrologic model	
GHS hydraulic conductivity§,#	10^{-4}–10^{-12} m/s
LHS hydraulic conductivity§,#	$5*10^{-7}$–10^{-12} m/s
TS hydraulic conductivity§,#	10^{-10}–10^{-12} m/s
IS hydraulic conductivity§,#	10^{-12} m/s
Hydraulic conductivity below B/D#,††	10^{-12} m/s
Porosity§	10%
Specific storage§§	10^{-10} m^{-1}
Fluid specific heat##	4200 J/kg K
Fluid density##	1000 kg/m^3

Note: † See Whipp et al., 2007 for parameter sources.

§ Freeze and Cherry, 1979, p. 29, 37.

Ingebritsen and Manning, 1999 and references therein.

†† B/D = Brittle-ductile transition

§§ Typical value, see Fetter, 1988, p. 106.

Average value from Lide, 1990, p. **6**-8.

The primary variable in the hydrologic model, the hydraulic conductivity (K), is specified for each lithostratigraphic unit and varied across a range of values measured in different rock types (Table DR1). The hydraulic conductivity decreases following a quasi-exponential function from the surface of the model to a minimum value at a depth of -7 km (Eqn. (DR1)). This is the approximate depth of the brittle-ductile transition in the models, below which rock permeability is thought to decrease to a low, constant value (Ingebritsen and Manning, 1999; Williams and Narasimhan, 1989). K is assigned across 1 km intervals from the mean elevation of ~3 km down to the constant value at -7 km. Elements above the mean elevation have a constant value of the maximum K for the given lithostratigraphic unit. The general equation used for K at depth is given by

$$\log_{10}(K) = \left(-n/d\right) * z + \log_{10}\left(K_{\max}\right), \qquad \text{(DR1)}$$

where K_{max} is the maximum K value for the unit, n is the number of orders of magnitude between K_{max} and the impermeable value, d is the thickness of the unit above the brittle-ductile transition (10 km), and z is the elevation of the depth interval relative to the mean elevation. The range of K values for the different lithostratigraphic units is listed in Table DR1.

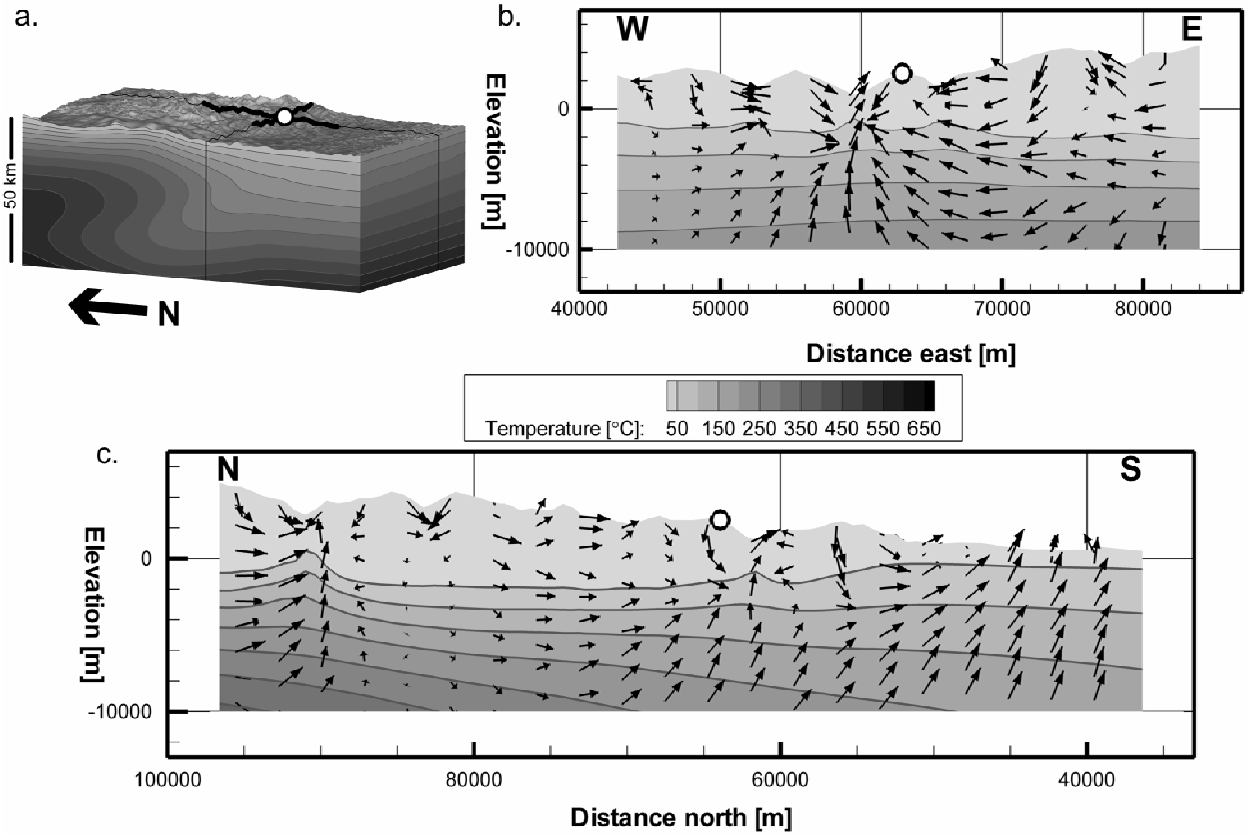

Figure DR2 – Vertical slices extracted from a fluid-advective thermokinematic model illustrating groundwater flow pathways. (a) 50 km thick thermokinematic model block with extracted slice locations (heavy black lines) and Nagi Lek data transect location (white circle). (b) West to east vertical slice through model to -10 km depth with schematic flow vectors and data transect location (white circle). Vectors illustrate fluid flow patterns affected by short wavelength topography, but the vector lengths have no meaning. (c) North to south slice through model with flow vectors and data transect location. Longer wavelength topography drives a broader circulation pattern with flow down from the Tibetan Plateau toward the Indian foreland. Downward fluid flow depresses the thermal gradient and upward flow compresses it, as shown by the near-surface isotherms.

Thermochronometer Age Prediction Model

Following the approach of Whipp et al. (2007), thermochronometer ages are calculated using predicted cooling histories for model points coincident with the AFT sample locations. Cooling histories are generated by tracking the temperature of samples from the surface back to different depths in the thermal model. Predicted AFT ages are calculated using the *Laslett et al.* (1987) kinetic annealing algorithm as implemented by *Ehlers et al.* (2003). Although other (multi-)kinetic models have been proposed, the data used in this study have no compositional data available and cooled extremely fast, and therefore do not warrant use of a multi-kinetic model.

Appendix B: Thermal Power Calculations

The observed thermal power is calculated using data from four hot springs in the Marsyandi River valley (samples MLB 51, 53, 55 and 58 in Tables 2 & 6 of Evans et al. (2004)). Because the hot springs are observed to be enriched in Ge relative to river waters, Evans et al. (2004) used a simple end-member mixing equation (Eqn. 1 of Evans et al., 2004) to calculate spring flux. The mixing equation is

$$F_W^{HS} = \frac{[Si]_{trib}}{[Si]_{HS}} \times \frac{\left(\frac{Ge}{Si}\right)_R - \left(\frac{Ge}{Si}\right)_{trib}}{\left(\frac{Ge}{Si}\right)_{HS} - \left(\frac{Ge}{Si}\right)_R}, \qquad \text{(DR2)}$$

where F_W^{HS} is the fraction of river discharge attributed to hot spring input, $[Si]_{trib}$ is the concentration of Si in surface waters unaffected by hot spring input, $[Si]_{HS}$ is the hot spring Si concentration, $(Ge/Si)_R$, $(Ge/Si)_{trib}$ and $(Ge/Si)_{HS}$ are the Ge/Si ratios of the river down stream of the springs, unaffected surface waters and hot springs, respectively. Unless otherwise noted, all other values are taken from Evans et al. (2004) and summarized in Table DR2. The equation used to calculate thermal power is the same as that used by Ehlers and Chapman (1999),

$$P = \frac{\partial m}{\partial t} c \left(T_w - T_g\right), \qquad \text{(DR3)}$$

where P is the thermal power, $\partial m/\partial t$ is the mass flow rate, c is the fluid specific heat and $T_w - T_g$ is the temperature difference between the hot spring water and the ground. The mass flow rate ($\partial m/\partial t$) is calculated as the product of F_W^{HS}, the river volume flux and density of water. The average temperature of the observed springs is used for the spring water temperature (T_w). For the average ground temperature (T_g), the average air temperature is calculated at the average elevation of the Marsyandi River basin (3442 m). The average elevation is used because the groundwater in the Marsyandi River valley is likely infiltrating from all points within the basin and in equilibrium with the air temperatures. The average air temperature is 3.9°C at 3442 m elevation. The calculated ground temperature at that elevation is 2.5°C warmer, to estimate the influence of excess solar insolation (Putnam and Chapman, 1996). The total observed thermal power of the Marsyandi River valley hot springs is 61.4 ± 36.3 MW, where the uncertainty reflects the standard deviation of $(Ge/Si)_{HS}$.

Thermal power is also calculated for each simulation using Eqn. (DR3) to compare to the observed value and constrain *K*. In the finite element model, only elements at the top surface with positive fluid velocity z-components contribute to the thermal power. The temperature gradient ($T_w - T_g$) is the thermal gradient across the element in the models. The mass flow rate ($\partial m/\partial t$) is the product of the flow velocity, area of the upper surface of the element and the fluid density. The element upper surface area is based on the 700 m x-y spacing of nodes in the model. To place bounds on the range of model thermal powers, it is calculated three different ways for each model: (1) All surface elements in the model contribute and are assumed to be flat lying, (2) all surface elements contribute and have a 30° hillslope angle, and (3) only elements within the Marsyandi River basin contribute and are assumed to be flat lying. Scenario (2) provides an upper bound for the thermal power calculations because it includes some elements outside of the Marsyandi River basin and uses a slope angle of 30° for the element surface area, which is higher than the average hillslope angle calculated from a 250 m DEM (~24°). Scenario (3) is likely to be an underestimate because it only includes elements within the Marsyandi River basin and assumes they are flat lying, underestimating the true surface area.

TABLE DR2. THERMAL POWER VALUES

Parameter	Value
Spring temperature*	51 °C
Average surface elevation†	3442 m
Calculated air temperature	3.9 °C
Calculated ground temperature	6.4 °C
Fluid-ground ΔT	44.6 °C
Si_{trib}§	155 μmol/kg
Si_{HS}*	1371 μmol/kg
$(Ge/Si)_R$§	2.2 μmol/mol
$(Ge/Si)_{trib}$§	0.7 μmol/mol
$(Ge/Si)_{HS}$*,#	109.03 μmol/mol
HS fraction*	0.1587%
River flux§	210 m^3/s
Volume flux*	330 L/s; 0.33 m^3/s
Water density	988.063 kg/m^3
Mass flow rate*	329.32 kg/s
Specific heat	4183 J/kg K
Thermal power	61.4 ± 36.3 MW

Note: * Recalculated from data of Evans et al. (2004).

† Calculated from 250 m DEM (see text).

§ Value from Evans et al. (2004).

Si weighted average.

References Cited

Bilham, R., Larson, K.M., Freymueller, J.T., Jouanne, F., Le Fort, P., Leturmy, P., Mugnier, J.L., Gamond, J.F., Glot, J.P., Martinod, J., Chaudury, N.L., Chitrakar, G.R., Gautam, U.P., Koirala, B.P., Pandey, M.R., Ranabhat, R., Sapkota, S.N., Shrestha, P.L., Thakuri, M.C., Timilsina, U.R., Tiwari, D.R., Vidal, G., Vigny, C., Galy, A., and de Voogd, B., 1997, GPS measurements of present-day convergence across the Nepal Himalaya: Nature, v. 386, p. 61-64.

Brooks, A.N., and Hughes, T.J.R., 1982, Streamline Upwind / Petrov-Galerkin formulations for convective dominated flows with particular emphasis on the incompressible Navier-Stokes Equations: Computer Methods in Applied Mechanics and Engineering, v. 32, p. 199-259.

Ehlers, T.A., and Chapman, D.S., 1999, Normal fault thermal regimes; conductive and hydrothermal heat transfer surrounding the Wasatch Fault, Utah: Tectonophysics, v. 312, p. 217-234.

Ehlers, T.A., Willett, S.D., Armstrong, P.A., and Chapman, D.S., 2003, Exhumation of the Central Wasatch Mountains, Utah: 2. Thermo-kinematics of exhumation and thermochronometer interpretation, Journal of Geophysical Research, Volume 108, p. 2173.

Evans, M.J., Derry, L.A., and France-Lanord, C., 2004, Geothermal fluxes of alkalinity in the Narayani river system of central Nepal: Geochemistry, Geophysics, Geosystems - G (super 3), v. 5, p. no.8, 21.

Fielding, E., Isacks, B., Barazangi, M., and Duncan, C.C., 1994, How flat is Tibet?: Geology, v. 22, p. 163-167.

Ingebritsen, S.E., and Manning, C.E., 1999, Geological implications of a permeability-depth curve for the continental crust: Geology, v. 27, p. 1107-1110.

Kohl, T., and Hopkirk, R.J., 1995, "FRACTure" a simulation code for forced fluid flow and transport in fractured, porous rock: Geothermics, v. 24, p. 333-343.

Larson, K.M., Buergmann, R., Bilham, R., and Freymueller, J.T., 1999, Kinematics of the India-Eurasia collision zone from GPS measurements: Journal of Geophysical Research, B, Solid Earth and Planets, v. 104, p. 1077-1093.

Laslett, G.M., Green, P.F., Duddy, I.R., and Gleadow, A.J.W., 1987, Thermal annealing of fission tracks in apatite: Chemical Geology; Isotope Geoscience Section, v. 65, p. 1-13.

Phillips, S.L., Igbene, A., Fair, J.A., Ozbek, H., and Tavan, M., 1981, A Technical Databook for Geothermal Energy Utilization, Lawrence Berkeley Laboratory, USA.

Putnam, S.N., and Chapman, D.S., 1996, A geothermal climate change observatory; first year results from Emigrant Pass in Northwest Utah: Journal of Geophysical Research, B, Solid Earth and Planets, v. 101, p. 21,877-21,890.

Smith, L., and Chapman, D.S., 1983, On the thermal effects of groundwater flow - 1. Regional scale systems: Journal of Geophysical Research, v. 88, p. 593-608.

Whipp, D.M., Jr., Ehlers, T.A., Blythe, A.E., Huntington, K.W., Hodges, K.V., and Burbank, D.W., 2007, Plio-Quaternary exhumation history of the central Nepalese Himalaya: 2. Thermokinematic and thermochronometer age prediction model: Tectonics, In press, doi:10.1029/2006TC001991.

Williams, C.F., and Narasimhan, T.N., 1989, Hydrogeologic constraints on heat flow along the San Andreas Fault; a testing of hypotheses: Earth and Planetary Science Letters, v. 92, p. 131-143.